First-principles based simulations of electronic transmission in ReS_2/WSe_2 and $ReS_2/MoSe_2$ type-II vdW heterointerfaces

Dipankar Saha[*†‡] and Saurabh Lodha [*]

Abstract

Electronic transmission in monolayer ReS_2 and ReS_2 based van der Waals (vdW) heterointerfaces are studied here. Since ReS_2/WSe_2 and $ReS_2/MoSe_2$ type-II vdW heterostructures are suitable for near infrared (NIR)/short-wave infrared (SWIR) photodetection, the role of interlayer coupling at the heterointerfaces is examined in this work. Besides, a detailed theoretical study is presented employing density functional theory (DFT) and nonequilibrium Green's function (NEGF) combination to analyse the transmission spectra of the two-port devices with ReS_2/WSe_2 and $ReS_2/MoSe_2$ channels and compare the near-equilibrium conductance values.

Single layer distorted 1T ReS_2 exhibits formation of parallel chains of 'Re'-'Re' bonds, leading to in-plane anisotropy. Owing to this structural anisotropy, the charge carrier transport is very much orientation dependent in ReS_2. Therefore, this work is further extended to investigate the role of clusterized 'Re' atoms in electronic transmission.

1 Introduction

In recent years significant progress in micro and nano photonics has been observed owing to the optoelectronic devices based on atomically thin two-dimensional (2D) layered materials and their vertical stacks [1, 2, 3, 4, 5, 6, 7, 8, 9, 10, 11, 12, 13, 14]. Such 2D materials can be metallic (graphene) or, semiconducting (e.g., black phosphorus, transition metal dichalcogenides (TMDs), etc.) or, a combination of both [15, 16, 17, 18, 19]. The vdW heterointerfaces formed with vertical stacking of 2D materials may exhibit compelling new properties which are significantly different from those of the participant materials [8, 20, 21]. Strong interlayer coupling and fast charge transfer across vdW interface are the

[*]Department of Electrical Engineering, Indian Institute of Technology Bombay, Mumbai-400076, India.

[†]Department of Electronics and Telecommunication Engineering, Indian Institute of Engineering Science and Technology Shibpur, Howrah-711103, India.

[‡]email: dipsah_etc@yahoo.co.in

1

key features which largely determine performance efficiency of the heterostructures [8, 9, 20, 22, 23]. In oder to design ultrafast NIR and SWIR photodetectors, a theoretical study exploring various possible combinations of group-6 and group-7 monolayer TMDs is presented in [20]. Among different combinations of type-II vdW heterostructures, it has been found that both ReS_2/WSe_2 and $ReS_2/MoSe_2$ emerge as suitable candidates with efficient generation, separation, and collection of charge carriers [20]. Howbeit, the effects of interlayer coupling on the electronic structures of ReS_2/WSe_2 and $ReS_2/MoSe_2$ were not captured in [20]. Moreover, to quantify the near-equilibrium conductance values of those heterointerfaces, a detailed analysis of electronic transmission through the ReS_2/WSe_2 and the $ReS_2/MoSe_2$ needs to be conducted.

Thus, in this work, considering band dispersions and electron difference density (EDD) calculations, first we try to investigate the role of interlayer coupling at the vdW heterojunctions. Next, utilizing NEGF along with DFT, we have shown the electronic transmission of two-port devices with the ReS_2/WSe_2 and the $ReS_2/MoSe_2$ channels and compared their conductance values at near-equilibrium.

Besides, we have also investigated the anisotropic carrier transmission of the group-7 constituent material, that is distorted 1T ReS_2. But for the group-6 TMDs (e.g., MoS_2, WS_2, $MoSe_2$, and WSe_2), because of the symmetric honeycomb structure of semiconducting 2H phase, such in-plane anisotropy is generally not expected [20, 24]. Furthermore, it is worth mentioning that orientation dependent electro-thermal transport in 2D layered materials can be useful for the purpose of designing low power, ultrathin next generation electronic devices [24, 25, 26, 27, 28, 29]. Among various 2D materials, in-plane anisotropy owing to structural transformation is seen in the 1T′ phase of the MoS_2 [24, 30]. Strong anisotropic conductance, due to clusterization of 'Mo' atoms along the transport direction, is reported in [24]. A similar trend can be seen in distorted 1T ReS_2, where the formation of parallel chains of 'Re'-'Re' bonds can lead to orientation dependent anisotropic transport [25]. As reported in [25], distorted 1T ReS_2 exhibits direction dependent I-V as well as transfer characteristics. Such experimental observation motivated us to explore the electronic properties of single layer distorted 1T ReS_2 and investigate the role of clusterized 'Re' atoms in carrier transmission.

2   Methodology

In order to coduct first-principles based DFT calculations, the software package "QuantumATK" was used [31, 32]. For all the unit cells and the supercells, computation of electronic structures and geometry optimizations were performed using the generalized gradient approximation (GGA) as exchange correlation along with the Perdew-Burke-Ernzerhof (PBE) functional [33]. Moreover, LCAO (linear combination of atomic orbitals) based numerical basis sets were utilized in this study to obtain results at the cost of reasonable computational load [24, 31].

To attain good accuracy of quantum transport and electronic structure calculations, the OPENMX (Open source package for Material eXplorer) code was used as the norm-conserving pseudopotentials [34, 35]. The basis sets for Mo, S, W, Se, and Re were taken as "s3p2d1", "s2p2d1", "s3p2d1", "s2p2d1", and "s3p2d1" respectively. Besides, the density mesh cut-off value was set to 200 Hartree and the k-points in Monkhorst-Pack grid were set to $9\times9\times1$ (X-Y-Z) for the unit cells and $9\times9\times3$ for the heterostructures. Sufficient vacuum was incorporated along the direction normal to the in-plane for the purpose of avoiding spurious interaction between periodic images. Furthermore, to include the effects of vdW interactions among different monolayers, the Grimme's dispersion correction (DFTD2) was employed [36].

Considering the two-port devices, transmission spectra along the channels were computed utilizing NEGF along with DFT. The k-points in Monkhorst-Pack grid were adopted as $1\times9\times150$ for the device calculations. Apart from that, in order to solve the Poisson's equation, Dirichlet boundary condition in the transport direction (Z direction) and periodic boundary conditions in the other two directions (X–Y directions) were assigned. In the framework of NEGF, taking into account the broadening matrices $\Gamma_{l,r}(E) = i[\Sigma_{l,r} - \Sigma_{l,r}^{\dagger}]$ for the left and the right electrodes (set by computing the self energy matrices Σ_l and Σ_r) [37, 38], the electronic transmission is calculated as,

$$T_e(E) = \text{Tr}[\Gamma_l(E)\, G(E)\, \Gamma_r(E)\, G^{\dagger}(E)] \,, \tag{1}$$

where $G(E)$ and $G^{\dagger}(E)$ denote retarded Green's function and advanced Green's function respectively [24, 37, 39].

3   Results and Discussion

Figure 1 illustrates a typical type-II vdW heterostructure formed with vertical stacking of group-6 and group-7 monolayer TMDs, as well as highlights its salient features [20]. Considering NIR/SWIR photodetection, near-direct bandgap, larger band offset values, and feasibility of integrating with flexible substrates make monolayer ReS_2 (group-7 TMD)/ monolayer WSe_2 (group-6 TMD) heterointerface a potentially promising candidate for the next generation ultrathin optoelectronic device [2, 9, 17, 20]. Even with the increase in number of layers of ReS_2 and WSe_2, we find that the near-direct type-II band alignment remains unaltered, hence ensuring efficient optical generation across the vdW interface [22]. Apart from that, monolayer ReS_2 (group-7 TMD)/ monolayer $MoSe_2$ (group-6 TMD) heterostructure can also be suitable for NIR/SWIR photodetection owing to its near-direct bandgap and superior optical absorption of the constituent $MoSe_2$ layer [20].

Figure 2 and 3 depict the electronic structures of ReS_2/WSe_2 and $ReS_2/MoSe_2$ considering element-wise contributions [40, 41, 42]. Both the projected density of states (DOS) plots exhibit type-II band alignments with energy gap values
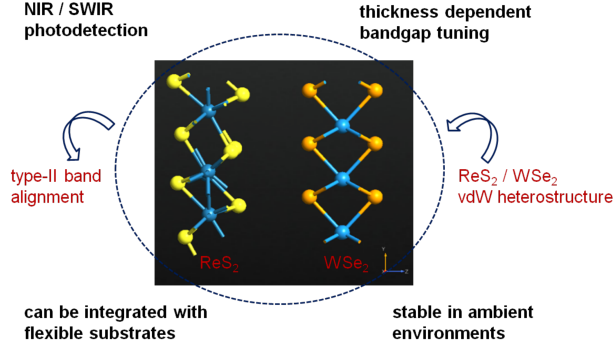
Figure 1: Vertical stacking of group-6 and group-7 monolayer TMDs to form a type-II vdW heterointerface (viz. ReS_2/WSe_2).

of 0.684 eV and 0.842 eV for the ReS_2/WSe_2 and the $ReS_2/MoSe_2$ heterostructures. Besides, the in-plane lattice constants and the equilibrium interlayer distance for the hexagonal vdW heterointerface of ReS_2/WSe_2 (Fig. 2 inset) are a=b= 6.600 Å and 3.49 Å respectively [20]. Those values for $ReS_2/MoSe_2$ interface (Fig. 3 inset) are a=b= 6.597 Å and 3.41 Å. [20].
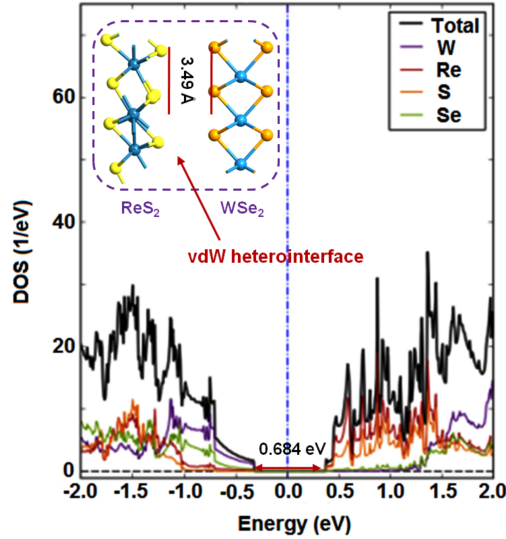

Figure 2: Projected DOS plots for ReS_2/WSe_2 vdW heterointerface.

In order to determine the effect of interlayer coupling, next we carry out a detailed analysis which emphasizes mainly on the band dispersions and the
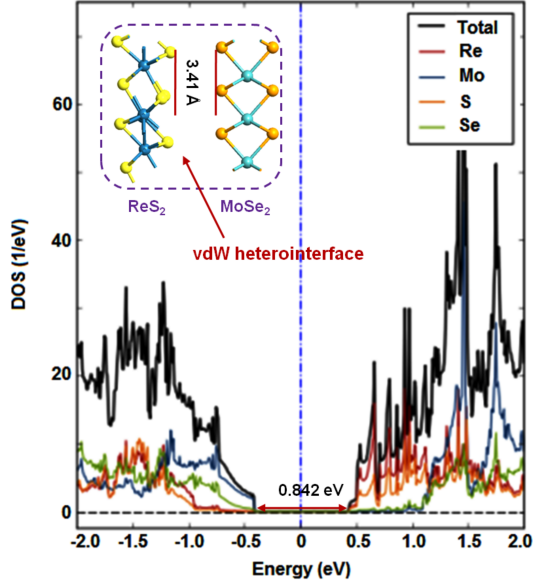
4

Figure 3: Projected DOS plots for $ReS_2/MoSe_2$ vdW heterointerface.

electron difference density (EDD) calculations of the heterointerfaces [43]. We consider the equilibrium interlayer distances of ReS_2/WSe_2 and $ReS_2/MoSe_2$ as the references (which are computed while optimizing the geometries utilizing LBFGS (Limited-memory Broyden Fletcher Goldfarb Shanno) algorithm). We also maintain the stacking patterns of the fully relaxed heterostructures same as those obtained form geometry optimization calculations. We then vary the interlayer distances (d_{int}), and compute band dispersions of the vdW heterostructures (Fig. S1(a) and S1(b)). The changes in indirect and direct bandgap (I_{gap} and D_{gap}) values, as we deviate from the equilibrium interlayer distances, are listed in Table 1.

I_{gap} and D_{gap} for ReS_2/WSe_2 are 0.68 eV and 0.83 eV, when the d_{int} is 3.49 Å (equilibrium interlayer distance). On the other hand, I_{gap} and D_{gap} for $ReS_2/MoSe_2$ are 0.84 eV and 0.98 eV, when the d_{int} is 3.41 Å (equilibrium interlayer distance). Now, as we shift the d_{int} around the equilibrium distances, we find that there are no noteworthy changes in band dispersions of ReS_2/WSe_2 and $ReS_2/MoSe_2$ (Fig. S1(a) and S1(b)), though the I_{gap} and the D_{gap} values do vary. We denote these changes as $|\Delta E_I|$ and $|\Delta E_D|$ (Table 1). Moreover, it is important to note that the variations in $|\Delta E_I|$ and $|\Delta E_D|$ are similar for the aforementioned type-II heterostructures.

Hence, we look into another important aspect, that is the EDD or the charge re-distribution between the constituent layers. As depicted in the cut plane diagrams of Fig. 4, negative and positive values of EDD indicate charge depletion

Table 1: Change in bandgap with the varying interlayer distances

interface	d_{int} (Å)	I_{gap} (eV)	D_{gap} (eV)	$|\Delta E_I|$ (eV)	$|\Delta E_D|$ (eV)
	2.69	0.80	0.89	0.12	0.06
ReS_2/WSe_2	3.49	0.68	0.83	0.00	0.00
	4.30	0.66	0.83	0.02	0.00
	5.10	0.66	0.82	0.02	0.01
	2.71	0.92	0.96	0.08	0.02
$ReS_2/MoSe_2$	3.41	0.84	0.98	0.00	0.00
	4.48	0.82	0.98	0.02	0.00
	5.18	0.81	0.97	0.03	0.01

and charge accumulation respectively. The EDD plot for ReS_2/WSe_2 (Fig. 4(a)) delineates minimum and maximum values of difference density as -0.29 and 0.2 Å^{-3}. Thus the corresponding average value is $\sim$ -0.04 Å^{-3}. On the other hand, EDD plot for $ReS_2/MoSe_2$ (Fig. 4(b)) shows minimum and maximum values of difference density as -0.29 and 0.79 Å^{-3}, with the average of $\sim$ 0.25 Å^{-3}. The larger average value of EDD for the $ReS_2/MoSe_2$ interface is essentially interpreting more charge distribution. Therefore, we can expect much stronger effect of interlayer coupling at the heterointerface of $ReS_2/MoSe_2$. In the following, we have further compared the electronic transmission in both the vdW heterointerfaces and observed a similar trend.

Next, to model the two-port devices, we take into account the geometry optimized vertical stacks of ReS_2/WSe_2 and $ReS_2/MoSe_2$ as illustrated in Fig. 2 and Fig. 3 (insets). As shown in Fig. 5, the group-7 and the group-6 TMD layers are extended to form the left and the right electrodes respectively. For the ReS_2/WSe_2 device, t_{left} (length of the left electrode) = t_{right} (length of the right electrode) is $\sim$ 6.60 Å. For the $ReS_2/MoSe_2$ device, that value is $\sim$ 6.59 Å. The length and the width of the channel region of ReS_2/WSe_2 two-port device are 6.658 nm and 1.143 nm (Fig. 5(a)). Considering the channel region of $ReS_2/MoSe_2$ two-port device, those values are 6.654 nm and 1.142 nm respectively (Fig. 5(b)). Besides, for those composite two-port device structures, the overlapping regions are maintained as $\sim$ 2.423 nm. It is worth mentioning that the mean absolute strain values on both the monolayer surfaces are 0.61% and 0.59% for ReS_2/WSe_2 and $ReS_2/MoSe_2$ channels [20].

Figure 6 shows the transmission spectra (zero bias) of the two-port devices, where we can observe that the transmission through $ReS_2/MoSe_2$ channel is slightly better than that in ReS_2/WSe_2 (cosidering a small energy range near
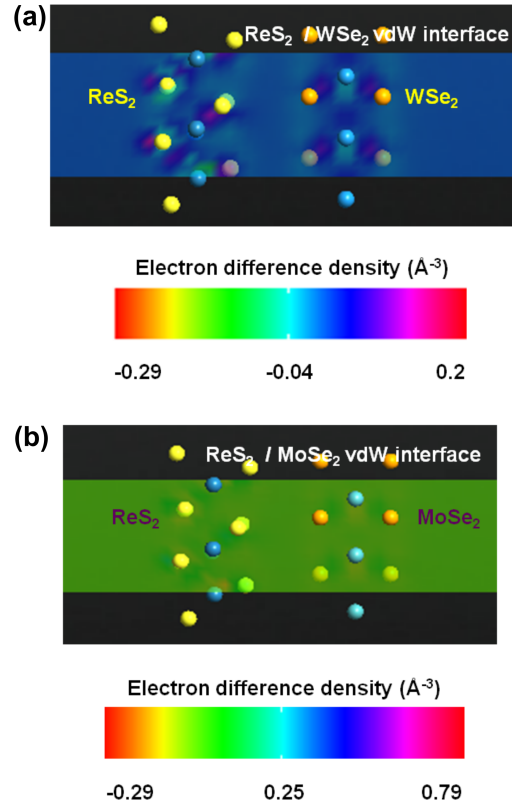
Figure 4: EDD plots showing charge re-distribution between the constituent layers of (a) ReS_2/WSe_2 and (b) $ReS_2/MoSe_2$.

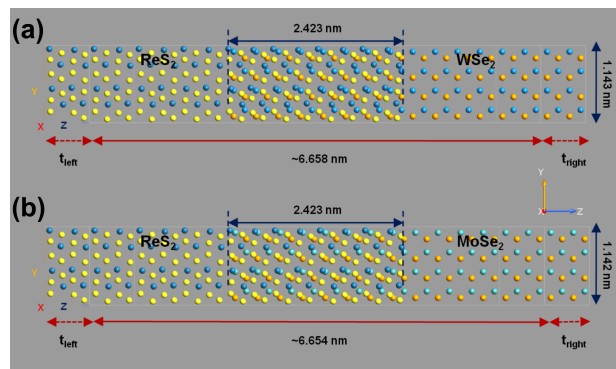Figure 5: Atomistic models of the two-port devices with (a) ReS_2/WSe_2 and (b) $ReS_2/MoSe_2$ channels.
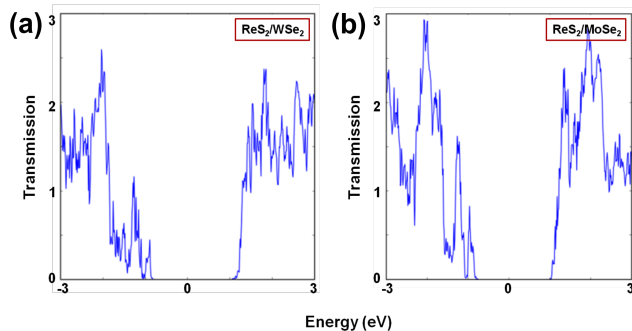
Figure 6: Transmission spectra of the two-port devices with (a) ReS_2/WSe_2 and (b) $ReS_2/MoSe_2$ channels.

the energy zero level). In order to quantify this we further calculate the near-equilibrium conductance and Seebeck coefficient values, as listed in Table 2. S and G_e denote the Seebeck coefficient and the electrical conductance, computed utilizing the linear response approximation ($\sim$ 300 K) [24, 38]. ΔE_F represents the shift in energy level from the energy zero. Moreover, the plots of Seebeck coefficients for the energy range of -3 eV to 3 eV are shown in Fig. S2. Similar to the trends of transmission spectra (Fig. 6), the G_e values listed Table 2 reinforce that the $ReS_2/MoSe_2$ channel is more conducive to the charge carrier transport.

Next, we have extended this theoretical study to demonstrate in-plane anisotropy and orientation dependant carrier transmission in single layer distorted 1T ReS_2. For the purpose of modeling the two-port devices with distorted 1T ReS_2 channels, we consider three different supercells viz. 'ReS_2 supercell1' (where the diamond-shaped (DS) 'Re' chains are perpendicular to the transport direction), 'ReS_2 supercell2' (where the DS 'Re' chains are parallel to the transport direction), and 'ReS_2 supercell3' (where the structure is obtained from the geometry optimized ReS_2/WSe_2 and the angle between a_1-b_1 and b_1-c_1 is $\sim$ 123°) [20, 25].

Figure 7 shows the atomistic models of the two-port devices with 'ReS_2 supercell1' (length = 4.588 nm and width = 1.135 nm) and 'ReS_2 supercell2' (length = 4.541 nm and width = 1.311 nm) channel regions. Figure 8 and 9 illustrate the electron density plots and zero bias transmission spectra of 'ReS_2 supercell1' and 'ReS_2 supercell2'. It is important to realize here that we have purposefully designed those supercell structures where the 'Re'-'Re' bonds are either parallel or perpendicular to the transport direction (Z direction). However, for single layer distorted 1T ReS_2, intrinsically the DS 'Re' chains form a certain angle with the [100]/[010] axis [20, 25]. Thus, as illustrated in Fig. 10(a), ReS_2 supercell3' (channel length = 4.620 nm and width = 1.143 nm) essentially exhibits the natural orientation of DS 'Re' chains.

8

Table 2: Details of near-equilibrium conductance values

two-port devices	ΔE_F (eV)	G_e (S)	S (V/K)
	0.9	2.906×10^{-9}	-0.0004686
	1.0	9.022×10^{-8}	-0.0002988
ReS_2/WSe_2	1.1	1.023×10^{-6}	-0.0001835
(length = 6.658 nm	1.2	8.563×10^{-6}	-0.0001511
width = 1.143 nm)	1.3	3.540×10^{-5}	-4.829×10^{-5}
	1.4	5.180×10^{-5}	-1.856×10^{-5}
	1.8	7.897×10^{-5}	-9.423×10^{-6}
	0.9	4.925×10^{-8}	-0.0004324
	1.0	1.396×10^{-6}	-0.0002594
$ReS_2/MoSe_2$	1.1	1.252×10^{-5}	-0.000103
(length = 6.654 nm	1.2	3.497×10^{-5}	-5.931×10^{-5}
width = 1.142 nm)	1.3	6.848×10^{-5}	-2.906×10^{-5}
	1.4	7.434×10^{-5}	-1.313×10^{-5}
	1.8	8.396×10^{-5}	-1.164×10^{-5}

Electron density plots of Fig. 8 depict how the valence electrons around 'Re' atoms are distributed across the channel regions. Apart from that, significant reduction in energy gap values can be observed for 'ReS$_2$ supercell1' and 'ReS$_2$ supercell2' (Fig. 9), owing to the large transmission states within the gap. Considering the transmission spectra as shown in Fig. 9, distinguishable transmission states within the range of 0.636 eV and 0.920 eV for 'ReS$_2$ supercell1' and 0.637 eV and 0.922 eV for 'ReS$_2$ supercell2', lower the energy gap values (~ 1.23 eV) of both the supercells.

However, the calculated energy gap for 'ReS$_2$ supercell3' (Fig. 10 (b)) is $\sim$ 1.37 eV. More importantly, this value is similar to the bandgap of distorted 1T ReS$_2$ unit cell [20]. It further reinforces that the 'ReS$_2$ supercell3' has the geometry where orientation of DS 'Re' chains as well as distribution of valence electrons around 'Re' atoms (Fig. 10(a)), reflects that of the natural single layer.
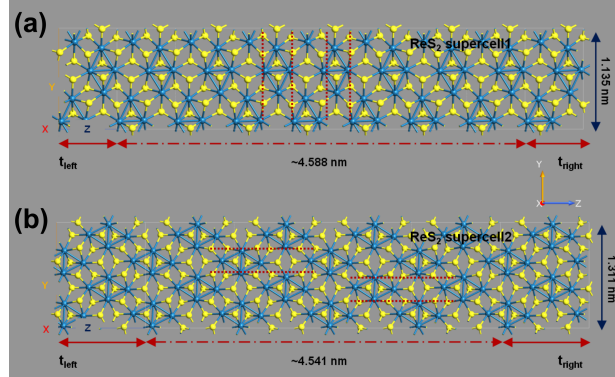
Figure 7: Atomistic models of (a) ReS_2 supercell1 and (b) ReS_2 supercell2, obtained by keeping the 'Re'-'Re' bonds are either perpendicular or parallel to the transport direction.
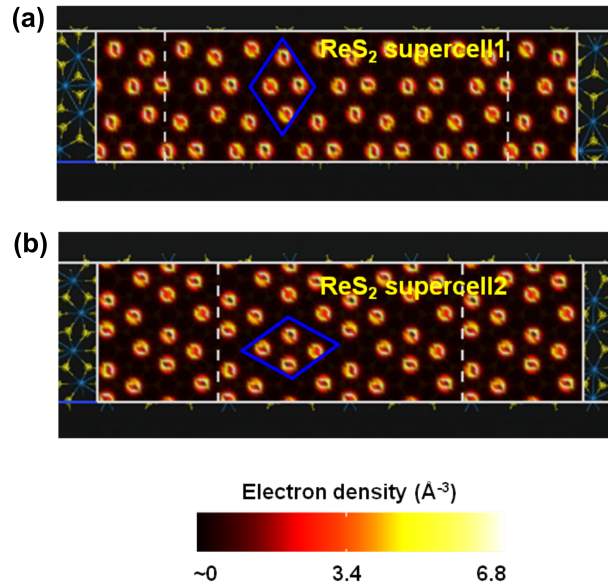

Figure 8: Electron density plots depicting the distribution of valence electrons around 'Re' atoms of ReS_2 supercell1 and ReS_2 supercell2.
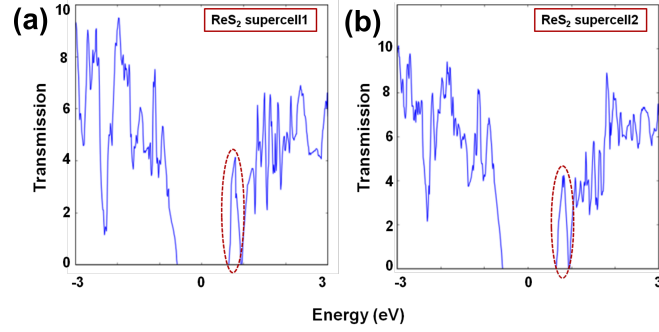
Figure 9: Transmission spectra (zero bias) of the two-port devices with (a) ReS_2 supercell1 and ReS_2 supercell2 channel regions.
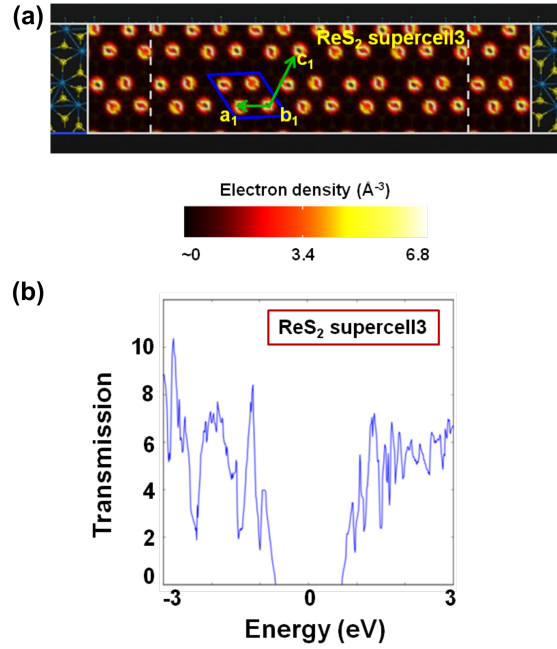

Figure 10: Plots illustrating the (a) electron density distribution around 'Re' atoms of ReS_2 supercell3 and (b) zero bias electronic transmission in two-port devices with ReS_2 supercell3 channel.

4   Conclusion

In this work, electronic transmission in single layer distorted 1T ReS_2 and distorted 1T ReS_2 based type-II vdW heterointerfaces are studied. We have demonstrated that the $ReS_2/MoSe_2$ heterostructure exhibits stronger effect of interlayer coupling at the heterointerface, owing to the larger average value of charge re-distribution between the constituent layers. Moreover, we have compared the electronic transmission through ReS_2/WSe_2 and $ReS_2/MoSe_2$ channels, and computed their near-equilibrium conductance values. We have found that the $ReS_2/MoSe_2$ channel is more conducive to the charge carrier transport. Apart from that, we have explored the in-plane anisotropy of the group-7 constituent material, that is the single layer distorted 1T ReS_2 and investigated the role of clusterized 'Re' atoms in electronic transmission. This study may further be extended for fewlayer ReS_2/WSe_2 and $ReS_2/MoSe_2$ channels, to explore their electronic properties and compare the near-equilibrium conductance values.

Acknowledgment

References

[1] F. H. L. Koppens, T. Mueller, Ph. Avouris, A. C. Ferrari, M. S. Vitiello and M. Polini, "Photodetectors based on graphene, other two-dimensional materials and hybrid systems," *Nature Nanotechnology*, 9, 780-793, 2014.

[2] Timothy C. Berkelbach and David R. Reichman, "Optical and Excitonic Properties of Atomically Thin Transition-Metal Dichalcogenides," *Annu. Rev. Condens. Matter Phys.*, 9, 379-396, 2018.

[3] The International Technology Roadmap For Semiconductors 2.0, "Outside System Connectivity," 2015.

[4] Oriol Lopez-Sanchez, Dominik Lembke, Metin Kayci, Aleksandra Radenovic, and Andras Kis, "Ultrasensitive photodetectors based on monolayer MoS_2," *Nature Nanotechnology*, 8, 497-501, 2013.

[5] Thorsten Deilmann and Kristian Sommer Thygesen, "Dark excitations in monolayer transition metal dichalcogenides," *Phys. Rev. B*, 96, 201113(R), 2017.

[6] Kartikey Thakar, Bablu Mukherjee, Sameer Grover, Naveen Kaushik, Mandar Deshmukh, and Saurabh Lodha, "Multilayer ReS_2 Photodetectors with Gate Tunability for High Responsivity and High-Speed Applications," *ACS Appl. Mater. Interfaces*, 10, 42, 36512-36522, 2018.

[7] Sayantan Ghosh, Abin Varghese, Kartikey Thakar, Sushovan Dhara, and Saurabh Lodha, "Enhanced responsivity and detectivity of fast WSe_2 phototransistor using electrostatically tunable in-plane lateral p-n homojunction," *Nature Communications*, 12, 3336, 2021.

[8] A. K. Geim and I. V. Grigorieva, "Van der Waals heterostructures," *Nature*, vol. 499, pages 419-425, 2013.

[9] C-H. Lee, G-H. Lee, A. M. van der Zande, W. Chen, Y. Li, M. Han, X. Cui, G. Arefe, C. Nuckolls, T. F. Heinz, J. Guo, J. Hone and P. Kim, "Atomically thin p-n junctions with van der Waals heterointerfaces," *Nature Nanotechnology*, vol. 9, 676-681, Sep. 2014, doi: 10.1038/NNANO.2014.150.

[10] M. M. Furchi, A. Pospischil, F. Libisch, J. Burgdörfer, and T. Mueller, "Photovoltaic Effect in an Electrically Tunable van der Waals Heterojunction," *Nano Lett.*, 14, 4785-4791, Jul. 2014, doi: 10.1021/nl501962c.

[11] Pulickel Ajayan, Philip Kim, and Kaustav Banerjee, "Two-dimensional van der Waals materials," *Physics Today*, 69, 9, 38, 2016.

[12] Long Yuan, Ting-Fung Chung, Agnieszka Kuc, Yan Wan, Yang Xu, Yong P. Chen, Thomas Heine, and Libai Huang, "Photocarrier generation from interlayer charge-transfer transitions in WS_2-graphene heterostructures," *Science Advances*, 4, 2, e1700324, 2018.

[13] Chenhao Jin, Eric Yue Ma, Ouri Karni, Emma C. Regan, Feng Wang, and Tony F. Heinz, "Ultrafast dynamics in van der Waals heterostructures," *Nature Nanotechnology*, 13, 994-1003, 2018.

[14] Zilong Wang, Patrick Altmann, Christoph Gadermaier, Yating Yang, Wei Li, Lavinia Ghirardini, Chiara Trovatello, Marco Finazzi, Lamberto Duò, Michele Celebrano, Run Long, Deji Akinwande, Oleg V. Prezhdo, Giulio Cerullo, and Stefano Dal Conte, "Phonon-Mediated Interlayer Charge Separation and Recombination in a $MoSe_2$/WSe_2 Heterostructure," *Nano Lett.*, 21, 5, 2165-2173, 2021.

[15] Fengnian Xia, Thomas Mueller, Yu-ming Lin, Alberto Valdes-Garcia, and Phaedon Avouris, "Ultrafast graphene photodetector," *Nature Nanotechnology*, 4, 839-843, 2009.

[16] Qiushi Guo, Andreas Pospischil, Maruf Bhuiyan, Hao Jiang, He Tian, Damon Farmer, Bingchen Deng, Cheng Li, Shu-Jen Han, Han Wang, Qiangfei Xia, Tso-Ping Ma, Thomas Mueller, and Fengnian Xia, "Black Phosphorus

Mid-Infrared Photodetectors with High Gain," *Nano Lett.*, 16, 7, 4648-4655, 2016.

[17] Mathieu Massicotte et al., "Dissociation of two-dimensional excitons in monolayer WSe_2," *Nature Comms.*, 9, 1633, 2018.

[18] Mohammed Alamri, Maogang Gong, Brent Cook, Ryan Goul, and Judy Z. Wu, "Plasmonic WS_2 Nanodiscs/Graphene van der Waals Heterostructure Photodetectors," *ACS Appl. Mater. Interfaces*, 11, 36, 33390-33398, 2019.

[19] Chulho Park, Ngoc Thanh Duong, Seungho Bang, Duc Anh Nguyen, Hye Min Oh, and Mun Seok Jeong, "Photovoltaic effect in a few-layer ReS_2/WSe_2 heterostructure," *Nanoscale*, 10, 20306, 2018.

[20] Dipankar Saha, Abin Varghese, and Saurabh Lodha, "Atomistic Modeling of van der Waals Heterostructures with Group-6 and Group-7 Monolayer Transition Metal Dichalcogenides for Near Infrared/Short-wave Infrared Photodetection," *ACS Appl. Nano Mater.*, 3, 820-829, 2020.

[21] Pranjal Kumar Gogoi, Yung-Chang Lin, Ryosuke Senga, Hannu-Pekka Komsa, Swee Liang Wong, Dongzhi Chi, Arkady V. Krasheninnikov, Lain-Jong Li, Mark B. H. Breese, Stephen J. Pennycook, Andrew T. S. Wee, and Kazu Suenaga, "Layer Rotation-Angle-Dependent Excitonic Absorption in van der Waals Heterostructures Revealed by Electron Energy Loss Spectroscopy," *ACS Nano*, 13, 8, 9541-9550, 2019.

[22] Abin Varghese, Dipankar Saha, Kartikey Thakar, Vishwas Jindal, Sayantan Ghosh, Nikhil V Medhekar, Sandip Ghosh, and Saurabh Lodha, "Near-Direct Bandgap WSe_2/ReS_2 Type-II pn Heterojunction for Enhanced Ultrafast Photodetection and High-Performance Photovoltaics," *Nano Lett.*, 20, 3, 1707-1717, 2020.

[23] Dinh Hoa Luong, Hyun Seok Lee, Guru Prakash Neupane, Shrawan Roy, Ganesh Ghimire, Jin Hee Lee, Quoc An Vu, and Young Hee Lee, "Tunneling Photocurrent Assisted by Interlayer Excitons in Staggered van der Waals Hetero-Bilayers," *Adv. Mater.*, 29, 1701512, 2017.

[24] Dipankar Saha and Santanu Mahapatra, "Anisotropic transport in 1T′ monolayer MoS_2 and its metal interfaces," *Physical Chemistry Chemical Physics*, 19, 10453-10461, 2017.

[25] Yung-Chang Lin, Hannu-Pekka Komsa, Chao-Hui Yeh, Torbjorn Bjorkman, Zheng-Yong Liang, Ching-Hwa Ho, Ying-Sheng Huang, Po-Wen Chiu, Arkady V. Krasheninnikov, and Kazu Suenaga, "Single-Layer ReS_2: Two-Dimensional Semiconductor with Tunable In-Plane Anisotropy," *ACS Nano*, vol. 9, no. 11, 11249-11257, 2015.

[26] Daniel A. Chenet, O. Burak Aslan, Pinshane Y. Huang, Chris Fan, Arend M. van der Zande, Tony F. Heinz, and James C. Hone, "In-Plane Anisotropy

in Mono- and Few-Layer ReS_2 Probed by Raman Spectroscopy and Scanning Transmission Electron Microscopy," *Nano Lett.*, 15, 5667-5672, 2015.

[27] Hyejin Jang, Christopher R. Ryder, Joshua D. Wood, Mark C. Hersam, and David G. Cahill, "3D Anisotropic Thermal Conductivity of Exfoliated Rhenium Disulfide," *Adv. Mater.*, 29, 1700650, 2017.

[28] Natasha Goyal, Narendra Parihar, Himani Jawa, Souvik Mahapatra, and Saurabh Lodha, "Accurate Threshold Voltage Reliability Evaluation of Thin Al_2O_3 Top-Gated Dielectric Black Phosphorous FETs Using Ultrafast Measurement Pulses," *ACS Appl. Mater. Interfaces*, 11, 26, 23673-23680, 2019.

[29] Mohammad Rahman, Kenneth Davey, and Shi-Zhang Qiao, "Advent of 2D Rhenium Disulfide (ReS_2): Fundamentals to Applications," *Adv. Funct. Mater*, 27, 1606129, 2017.

[30] Manish Chhowalla, Hyeon Suk Shin, Goki Eda, Lain-Jong Li, Kian Ping Loh and Hua Zhang, "The chemistry of two-dimensional layered transition metal dichalcogenide nanosheets," *Nature Chemistry*, vol. 5, Aprl. 2013.

[31] QuantumATK version 2018.06, Synopsys QuantumATK, Available at https://www.synopsys.com/silicon/quantumatk.html.

[32] Søren Smidstrup et al., "QuantumATK: an integrated platform of electronic and atomic-scale modelling tools," *J. Phys.: Condens. Matter*, 32, 015901, 2020.

[33] J. P. Perdew, K. Burke, and M. Ernzerhof, "Generalized Gradient Approximation Made Simple," *Phys. Rev. Letters*, vol. 77, no. 18, 3865-3868, Oct. 1996, https://doi.org/10.1103/PhysRevLett.77.3865.

[34] T. Ozaki, "Variationally optimized atomic orbitals for large-scale electronic structures," *Phys. Rev. B*, 67, 155108, Aprl. 2003, doi: 10.1103/PhysRevB.67.155108.

[35] T. Ozaki and H. Kino, "Numerical atomic basis orbitals from H to Kr," *Phys. Rev. B*, 69, 195113, May 2004, doi: 10.1103/PhysRevB.69.195113.

[36] S. Grimme, "Semiempirical GGA-type density functional constructed with a long-range dispersion correction," *J. Comput. Chem.*, vol. 27, no. 15, pp. 1787-1799, 2006.

[37] T. Markussen, A-P. Jauho, and M. Brandbyge, "Electron and phonon transport in silicon nanowires: Atomistic approach to thermoelectric properties," *Phys. Rev. B* 79, 035415, 2009.

[38] D. Saha and S. Mahapatra, "Theoretical insights on the electro-thermal transport properties of monolayer MoS_2 with line defects," *J. Appl. Phys.*, 119, 134304, Aprl. 2016, http://dx.doi.org/10.1063/1.4945582.

[39] M. Brandbyge, J-L. Mozos, P. Ordejón, J. Taylor, and K. Stokbro, "Density-functional method for nonequilibrium electron transport," *Phys. Rev. B*, 65, 165401, March 2002, doi: 10.1103/PhysRevB.65.165401.

[40] R. W. G. Wyckoff, "Crystal structures," 1, 1963.

[41] W. J. Schutte, J.L. De Boer, and F. Jellinek, "Crystal structures of tungsten disulfide and diselenide," *Journal of Solid State Chemistry*, 70, 2, 207-209, 1987.

[42] Kristin Persson, "Materials Data on ReS$_2$ (SG:2) by Materials Project," , United States, doi:10.17188/1276430.

[43] Zhiming Shi, Xinjiang Wang, Yuanhui Sun, Yawen Li, and Lijun Zhang, "Interlayer coupling in two-dimensional semiconductor materials," *Semicond. Sci. Technol.*, 33, 093001, 2018.

Supporting Information

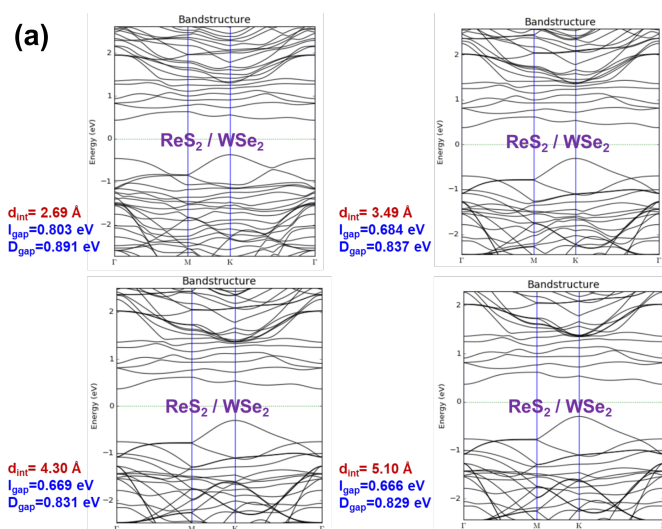**Band dispersions of the ReS$_2$/WSe$_2$ and ReS$_2$/MoSe$_2$ vdW heterointerfaces**

Figure S1 (a) : Band dispersions of the ReS$_2$/WSe$_2$ heterostructure with the varying interlayer distances.

(b)
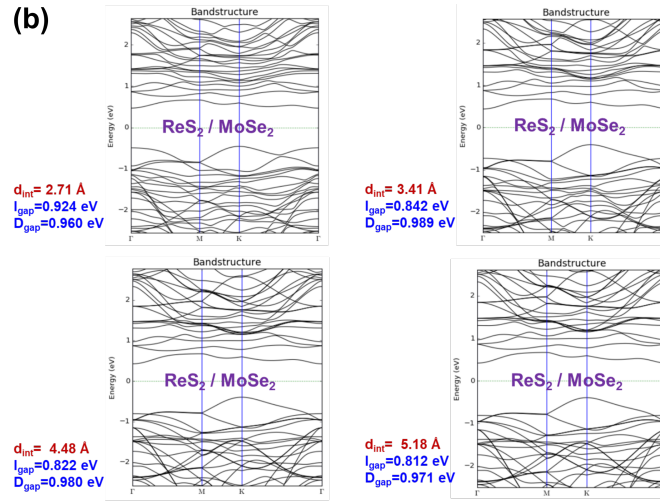

Figure S1 (b) : Band dispersions of the $ReS_2/MoSe_2$ heterostructure with the varying interlayer distances.

Seebeck coefficients plots (energy range of -3 eV to 3 eV)

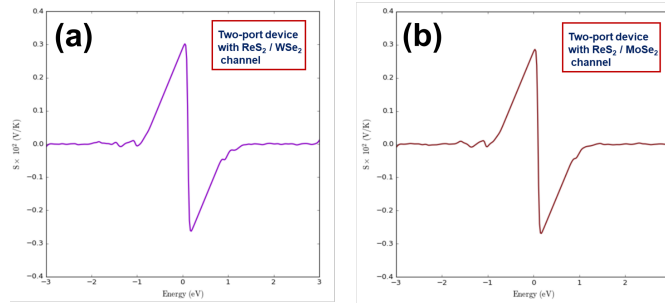Figure S2 : Seebeck coefficient plots of the two-port devices with (a) ReS_2/WSe_2 and (b) $ReS_2/MoSe_2$ channels.